Soft Matter

A Simple Landscape of Metastable State Energies for Two-Dimensional Cellular Matter

Journal:	*Soft Matter*
Manuscript ID	SM-ART-09-2018-001921.R1
Article Type:	Paper
Date Submitted by the Author:	03-Dec-2018
Complete List of Authors:	Kim, Sangwoo; University of Illinois, Mechanical Science and Engineering Hilgenfeldt, Sascha; University of Illinois, Mechanical Science and Engineering

Journal Name

ARTICLE TYPE

Cite this: DOI: 10.1039/xxxxxxxxxx

A Simple Landscape of Metastable State Energies for Two-Dimensional Cellular Matter†

Sangwoo Kim and Sascha Hilgenfeldt*

Received Date
Accepted Date

DOI: 10.1039/xxxxxxxxxx

www.rsc.org/journalname

The mechanical behavior of cellular matter in two dimensions can be inferred from geometric information near its energetic ground state. Here it is shown that the much larger set of all metastable state energies is universally described by a systematic expansion in moments of the joint probability distribution of size (area) and topology (number of neighbors). The approach captures bounds to the entire range of metastable state energies and quantitatively identifies any such state. The resulting energy landscape is invariant across different classes of energy functionals, across simulation techniques, and across system polydispersities. The theory also finds a threshold in tissue adhesion beyond which no metastable states are possible. Mechanical properties of cellular matter in biological and technological applications can thus be identified by visual information only.

1 Introduction

Two-dimensional Cellular Matter consists of domains (units like cells, drops, or bubbles, typically in single layers) that tile the plane with only a small fraction of continuous phase between them. These systems are found across fields and across length-scales from the microstructure of metals and biological tissues to geological formations[1–3]. Geometrically, such materials are patterns of polygons (Fig. 1a); while ordered crystals are important special cases[4–6], disordered arrangements of domains are much more commonly encountered. Ground states of mechanical energy in these systems have been shown to undergo a transition from rigid/solid to floppy/fluid states[7–9], which can be detected through geometric properties of the domains, particularly the perimeter-to-area ratio. Alternatively, such disordered ground states can also be characterized by particular correlations between the distributions of domain size and domain topologies[10,11]. Beyond the ground states, cellular systems inhabit a complex energy landscape of metastable states. In this work, a simple and universal expression for the metastable state energies is developed, with statistical moments of domain sizes and topologies as variables. This amounts to formulating a general linear continuum mechanics for inelastic deformations, quantifiable from morphological traits visible e.g. in tissue images.

A global energy minimum, if it exists at all in disordered systems[13], is very hard to determine (even in 2D foams, the only mathematically proven ground state is the monodisperse honeycomb[14]). Nevertheless, various annealing strategies in simulations find consistent low-energy states, which we call "(disordered) ground states" here. Often, however, a cellular material is only known to be in a *local* energy minimum, i.e., a metastable state (MS) somewhere above the ground state energy. The complex MS landscape is analogous to inherent structure networks in models of packings and liquids[15,16], and related to *jammed* states[17,18], as the system requires finite stress to move from one MS to another. Note that, while a small uncertainty is inherent in the energy value of the heuristically defined disordered ground states, the energies of metastable states discussed in the present work are larger by a significantly greater amount. Conversely,

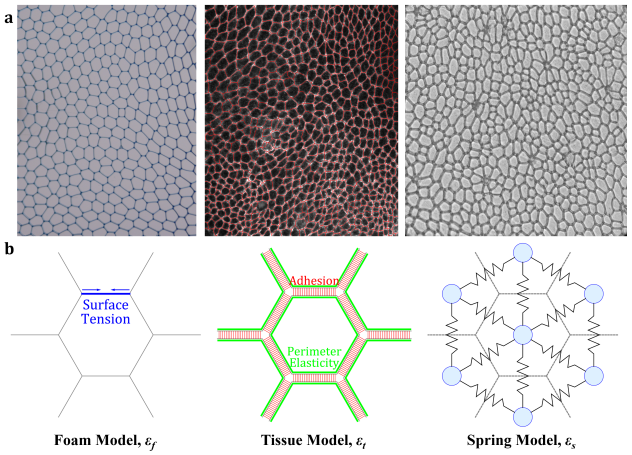

Fig. 1 Cellular Matter in 2D. a, Examples of cellular systems encountered in nature[12]: foam, *Drosophila* wing epithelial tissue, *Cucumis* epidermal tissue. **b**, Schematics of the energy functional elements in foam (constant tension), tissue (perimeter elasticity and adhesion), and spring (Hookean elasticity) model systems.

Mechanical Science and Engineering, University of Illinois at Urbana-Champaign. E-mail: sascha@illinois.edu

† Electronic Supplementary Information (ESI) available

significantly lower energies can only be obtained by introducing large-scale correlations into the system, e.g. spatially ordering the domains of a polydisperse system by size. Such a pattern is statistically extremely unlikely, and is not disordered.

In very recent work, the authors characterized the energies of topologically adjacent metastable states through the lengths of particular edges[19]; similar correlations were discovered in 3D tissue simulations as well[20]. The present work does not make use of this results, but focuses on the statistics of the areas A_i and topologies (number of neighbors) n_i of the individual domains, which can be measured much more robustly than edge lengths. We show that this description dramatically simplifies the energy landscape and allows extraction of MS energy information *from a snapshot of the structure only*.

2 Simulation of Cellular Matter Energy

2.1 Mechanical Energy Functionals

As we discuss static or quasi-static states of cellular matter, we exclude dynamical or dissipative effects, while covering a variety of elastic effects in a general mechanical energy functional. In this functional, we further assume that (i) the systems are composed of domains with equal properties, (ii) energy contributions from the (small) continuous phase fraction are negligible, and (iii) contributions from the bulk phase are dominated by the interfaces. The latter implies that interaction energy between domains can be equally partitioned between neighbors, so that the system energy is additive over domains i. Item (iii) also enforces constant areas A_i to exclude bulk contributions. Under these assumptions, the remaining, interface-dominated energy in 2D can be systematically expanded to first and second order in domain perimeters P_i, yielding[19]

$$\varepsilon_f = \frac{1}{6N\mathscr{L}_0}\sum_i P_i\,, \tag{1}$$

$$\varepsilon_t = \frac{1}{6N\mathscr{L}_0}\left(\sum_i \frac{(P_i-P_{i,0})^2}{P_{i,0}} - \gamma\sum_i P_i\right). \tag{2}$$

The former corresponds to foams and the latter to common tissue models[7,9,21], cf. Fig. 1b. The average energy ε of N domains is normalized by the edge length $\mathscr{L}_0$ of a regular hexagon of the average area $\bar{A}=A_{tot}/N$, which we set to $\bar{A}=1$ without loss of generality. In ε_t, $P_{i,0}$ is the equilibrium perimeter of individual domains, set to the equivalent circle perimeter $2\sqrt{\pi A_i}$ (a different choice merely rescales the functional), and $\gamma>0$ is a dimensionless adhesion strength. Loss of rigidity of the ground state occurs for $\gamma>\gamma_c\approx 0.12$[22] analogous to a critical shape index[7,23]. For all functionals, we explore samples of a wide range of polydispersities.

It is convenient for a common treatment of all functionals to translate ε_t to an equivalent foam energy $\varepsilon_f^* = \frac{1}{6N\mathscr{L}_0}\sum_i P_i^*$, summing domain perimeters P_i^* in the metastable tissue states (even though these are not equilibria under ε_f). The Supplementary Information shows in detail how ε_t can be obtained reliably from ε_f^*, i.e., there is an accurate functional relation $\varepsilon_t(\gamma,\varepsilon_f^*)$.

To probe the generality of our results, limited simulations were also performed for a very different energy functional, in order to assess whether the results carry over to systems where a domain geometry can be constructed, but does not originally determine energy: We model a set of N point objects confined to area A_{tot} interacting by springs of rest length $d_{0,ij}=r_{0,i}+r_{0,j}$, mimicking sticky elastic objects of undeformed size $r_{0,j}$. These sizes are obtained as equivalent circle radii of areas A_i, with $\sum_i^N A_i = A_{tot}$ as before. Assuming harmonic spring energies, this yields

$$\varepsilon_s = \frac{1}{6N\mathscr{L}_0^2}\sum_i\sum_j^{n.n.}(d_{ij}-d_{0,ij})^2\,, \tag{3}$$

where d_{ij} is the actual distance between object i and j and the j sum is over nearest neighbors of i (Fig. 1b). After finding local equilibrium positions of the point objects, a Voronoi tiling is constructed, whose total edge length again yields a proxy foam energy ε_f^*. Varying the width of the distribution of the $r_{0,i}$ gives access to a range of domain polydispersities.

2.2 Simulation Methods

Using the foam energy ε_f and the tissue energy ε_t (with various γ values), we generate a large number of metastable mechanical equilibrium states employing Surface Evolver (SE), a program specialized for this task[24]. As initial configurations for SE simulations, N Voronoi cells based on different types of point processes are constructed in a rectangle of area A_{tot} with periodic boundary conditions: (1) a perturbed lattice algorithm[22,25] using random displacements of the points in a regular triangular lattice; (2) Lloyd's algorithm[26], which reduces disorder by regularizing Voronoi patterns; and (3) an excluded-volume algorithm[27], where the Voronoi cells have hard-core exclusion areas. Each point process has a control parameter adjusting the degree of disorder; typically the number of domains is $N=400$ or 900 per sample, but larger simulations have been run and were in agreement with the results shown. Target values for domain areas A_i are generated from a gamma distribution with desired polydispersity c_A and assigned to individual cells by a combination of random and/or systematic protocols (other shapes of area distributions yield unchanged results in the range of c_A considered in this work). SE then displaces vertices in order to minimize the given energy functional; the program provides various tools for iterations towards the minimum and check of convergence. We use nonlinear edge representations to allow for the degrees of freedom of curved edges. If in the process of minimization an edge between domains shrinks to negligible length (a four-way edge junction forms), this indicates an unstable state, and SE performs a T1 transition. This repeats until a MS is found; alternatively, further MS are found through deliberate induction of non-spontaneous T1 transitions. The combined results of many simulation samples delineate the MS region in a complex energy landscape. Degenerate ground states of ε_t ("floppy" states) are characterized by a dramatic decrease of the energy to zero within the precision of the simulations. Overall, we analyze >200,000 MS and their statistical properties across polydispersities and energy functionals. For further details on different simulation pro-

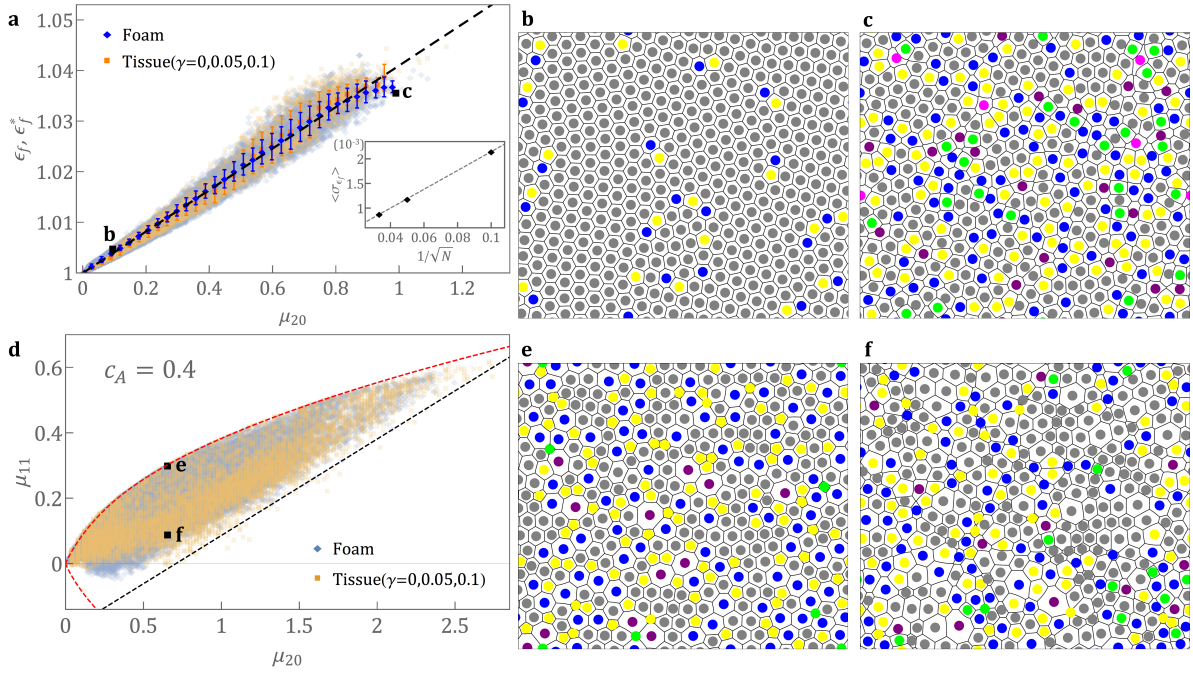

Fig. 2 Metastable state parameter dependences in foams and tissues. **a**, Linear correlation for monodisperse systems between (equivalent) foam energy (ε_f,ε_f^*) and defect density μ_{20}; the dashed line is the least square fit of empirical data with slope M_{20}. Error bars on binned data are standard deviations. Inset: The averaged standard deviation of ε_f over all bins decays as $1/\sqrt{N}$. **b, c**, Monodisperse structures ($N = 400$) at defect densities of $\mu_{20} = 0.095$ (low energy) and $\mu_{20} = 0.99$ (high energy), respectively; these states are also indicated in **a**. Domains are color-coded by topology, green: $n = 4$, yellow: $n = 5$, gray: $n = 6$, blue: $n = 7$, purple: $n = 8$, pink: $n = 9$. **d**, Polydisperse MS occupy a finite region in the $\mu_{20} - \mu_{11}$ plane, delineated by the analytical curves for maximum covariance $\pm\mu_{11}^{max}(\mu_{20})$ (red dashed) and maximum energy ε_f^{max} (black dashed). **e, f** Two MS for $c_A = 0.4$ with equal $\mu_{20} = 0.655$, but different covariance: **e**, $\mu_{11} = 0.297, \varepsilon_f = 0.985$ (low energy) and **f**, $\mu_{11} = 0.085, \varepsilon_f = 1.014$ (high energy).

tocols and the independence of our results on the algorithms see the Supplementary Information.

3 Monodisperse Systems

Considering *monodisperse* foam first, we expect any topological defects in a MS to indicate higher foam energy (as the regular honeycomb is the ground state), see Fig. 2b,c. Indeed, ε_f is found to increase linearly with the topology variance, $\mu_{20} \equiv (1/N)\sum_i (n_i - 6)^2$, as shown in Fig. 2a, i.e.,

$$\varepsilon_f^{mono}(\mu_{20}) = \varepsilon_0 + M_{20}\mu_{20}\,. \tag{4}$$

By definition, $\varepsilon_0 = 1$; we find the "modulus" value $M_{20} \approx 0.041$. Surprisingly, the linear relation is valid for the entire realizable range of μ_{20}: any attempt to construct a MS with $\mu_{20} > \mu_{20}^{max} \approx 1.0$ invariably produces unstable states, i.e., states undergoing spontaneous neighbor-change T1 relaxations [19,20,28] whose topological changes lead to smaller μ_{20} (cf. Materials and Methods). Because of (4), this also means MS energy is bounded by $\varepsilon_f^{max} \approx 1.045$. Domains in a configuration with $\mu_{20} \sim 1$ carry, on average, a topological charge of ± 1 [29], which can be conjectured as a threshold for the proliferation of unstable states that have to relax to lower-energy MS [30]. Note that Fig. 2a depicts *all* individual sample energies (in gray) – even the most extreme variation of ε_f from the mean is moderate, while the standard deviation (error bars) is much tighter and decays as $1/\sqrt{N}$ (inset), as expected from independently sampled values. For large enough sets of domains, the simple prediction (4) thus becomes very accurate.

Extensive simulations of MS tissue energies ε_t in monodisperse samples, when rescaled to ε_f^*, do not just qualitatively reproduce these results, but they prove quantitatively indistinguishable from the foam results (Fig. 2a). This holds independent of the adhesion parameter γ, as long as the system is rigid/solid ($\gamma < \gamma_c$). Thus, it is not necessary to know the value of γ in order to classify the MS energy of a tissue state. The slope M_{20} of (4) can be rationalized by analytically computing the energy change from elementary perturbations of the honeycomb lattice (see Supplementary Information). Performing either one or two elementary T1 operations from this ground state, one obtains two different predictions $M_{20}^{(1)} \approx 0.031$ and $M_{20}^{(2)} \approx 0.045$, respectively, which bracket the empirical value of M_{20}.

4 Polydisperse Systems

It is easy to convince oneself that knowing μ_{20} in a *polydisperse* system is not sufficient to predict its energy (see Fig. 2e,f for a counterexample). To generalize the theoretical approach to the polydisperse case, we model foam energy as a functional of the joint probability distribution $p(n,A)$ of topologies and sizes. All information about this distribution is contained in its moments μ_{ij} [31]. The 0^{th} and 1^{st} moments are trivial ($\mu_{00} = 1, \mu_{01} = \bar{A} = 1, \mu_{10} = \bar{n} = 6$). The simplest leading-order expansion of ε_f is then the linear combination

$$\varepsilon_f = \varepsilon_0 + M_{20}\mu_{20} + M_{11}\mu_{11} + M_{02}\mu_{02}\,. \tag{5}$$

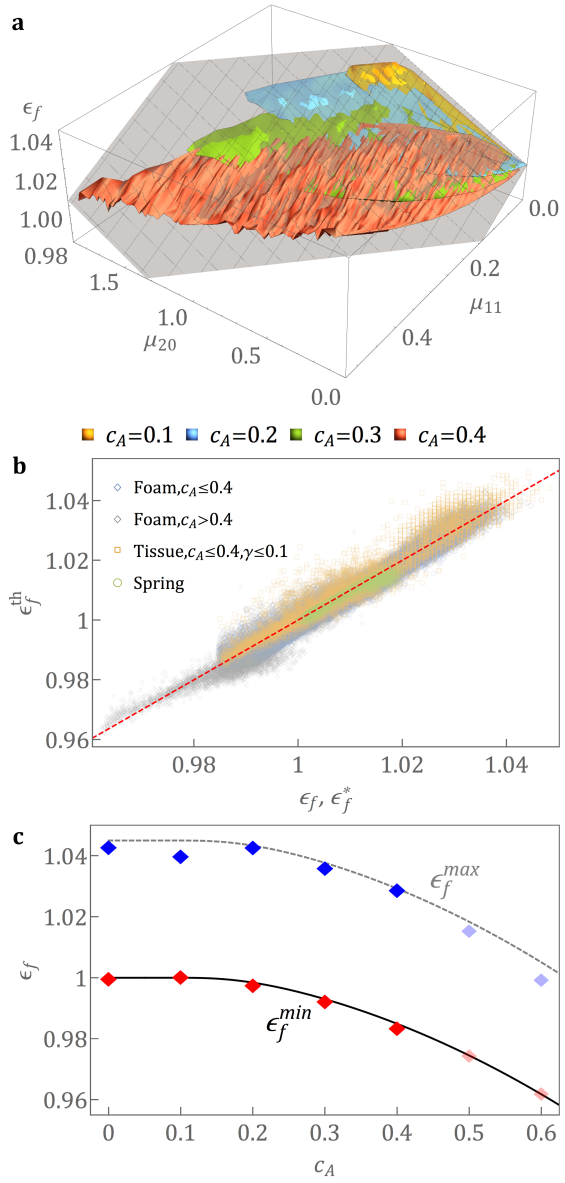

Fig. 3 Linear theory of metastable state mechanical energy. **a**, Planar energy landscape $\varepsilon_f(\mu_{20},\mu_{11})$ of binned foam simulation data of various polydispersities, compared with the universal prediction ε_f^{th} (gray plane) from (8). **b**, Direct comparison of ε_f^{th} with $(\varepsilon_f,\varepsilon_f^*)$ simulation data from individual foam, tissue, and spring system samples (red dashed line indicates perfect agreement). **c**, The lowest and highest sample MS energies from foam simulations (red and blue symbols, respectively) are well approximated by the estimates ε_f^{min}, ε_f^{max} (lines), even beyond the nominal range of validity $c_A \lesssim 0.45$.

Here, $\mu_{11} \equiv (1/N)\sum_i (n_i-\bar{n})(A_i-\bar{A})$ is the covariance and μ_{02} the area variance; we use $c_A = \mu_{02}^{1/2}$ as a handy polydispersity measure. We first observe that a MS with $n_i = 6$ for all i (and thus $\mu_{20} = 0$, $\mu_{11} = 0$) can be maintained up to a maximum polydispersity $c_A^{max} \approx 0.45$, while leaving the honeycomb energy $\varepsilon_0 = 1$ strictly invariant (see Supplementary Information). If (5) holds for all states, $M_{02} = 0$ is thus required.

Figure 2d shows (for the example of $c_A = 0.4$) that the simulated MS occupy only a finite region in $\mu_{20} - \mu_{11}$ space, but the variation of μ_{11} is a crucial factor co-determining the MS energy. For large μ_{11}, as in Fig. 2e, topologies and areas are matched and the energy is relatively low, while a mismatch of n_i and A_i leads to much higher energy (Fig. 2f): to accommodate large n_i for small A_i or vice versa, cells must deform and increase their perimeters and thus ε_f.

To make progress in understanding both the boundaries of the region of MS and the accompanying energies, we use a normal approximation to the area distribution that in the ground state yields an analytical prediction of $\mu_{20} = f_{gs}(c_A)$ [10]. For the present case of MS with variable μ_{20} at a given c_A, we parametrize this relation with an effective polydispersity x, i.e.,

$$\mu_{20} = f_{gs}(x) = \sum_{n=1}^{4} (2n-1)\,\mathrm{erfc}\left[\frac{\beta}{x}(2n-1)\right] \qquad (6)$$

where $\beta \approx 0.206$ is a constant. The maximum covariance (best possible match of n_i and A_i) follows explicitly,

$$\mu_{11}^{max}(x) = c_A \sum_{n=1}^{4} \sqrt{\frac{2}{\pi}} \exp\left[-\frac{\beta^2}{x^2}(2n-1)^2\right], \qquad (7)$$

see the Supplementary Information for the steps of the derivation. As shown in Fig. 2d, the parametric equation (6), (7) very accurately describes the region boundary $\mu_{11}^{max}(\mu_{20})$, while $-\mu_{11}^{max}$ is a lower bound. Furthermore, this relation implies that at the energy minimum of the ground state ($d\varepsilon_f = 0$, $x = c_A$), we have $d\mu_{20}/dx = k\,d\mu_{11}^{max}/dx$ with $k = -1/(\sqrt{2}\beta) \approx -3.43$. Extending the validity of the latter relation to the entire $\mu_{20} - \mu_{11}$ region, it implies, together with (5), the very simple prediction $M_{11} = kM_{20} \approx -0.141$.

5 A universal metastable state theory

Our ansatz has thus yielded a universal theoretical expression, valid for all polydispersities $c_A \lesssim c_A^{max}$, for the metastable state energies of a foam,

$$\varepsilon_f^{th} = 1 + 0.041\mu_{20} - 0.141\mu_{11}\,. \qquad (8)$$

Checked against all foam data, the agreement is very good (Fig. 3a), even for most samples with polydispersities beyond the nominal range (Fig. 3b). Again, the energies ε_t from tissue simulations with $\gamma < \gamma_c$, converted to ε_f^*, agree with this formula to the same degree of accuracy as the foams, and so do the simulations using spring energy ε_s (Fig. 3b). The quality of agreement is also unaffected by the value of the polydispersity.

Less extensive simulations tentatively support the validity for other energy functionals, such as those including area elasticity [21,32]. The approach will have to be modified, however, when considering systems that, while not fluid, possess inherent activity that leads to fluctuations of shape and/or of the area fraction of continuous phase [33]. Such structural changes will cause rearrangements in high-energy metastable states (which are likely to have short-edge domain boundaries and very small energy barriers [19]) and reduce the probability of their presence, altering the statistics and restricting the accessible MS region of phase space. Conversely, activity does not automatically invalidate the present approach – in many biological tissues, contractility is important

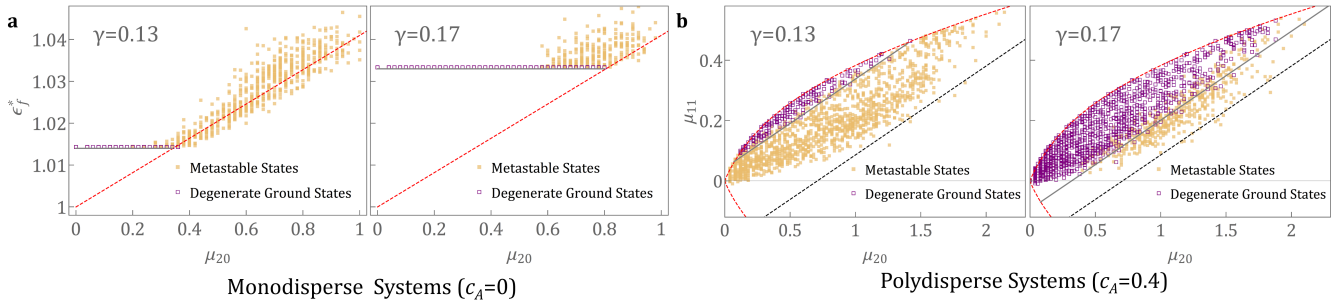

Fig. 4 Metastable states and loss of rigidity. **a**, Monodiperse tissue systems with $\gamma = 0.13$ (left) and $\gamma = 0.17$ (right) show degenerate ground states (floppy mechanics, purple) with flat $\varepsilon_f^*(\mu_{20}) = \varepsilon_{f,c}^*$ (gray solid line). They coexist with metastable states (orange) conforming to the MS energy prediction (red dashed line). **b**, Polydisperse systems with $c_A = 0.4$ for the same γ values. The region of floppy states lies beyond the line $\varepsilon_f^* = \varepsilon_{f,c}^*$ (gray solid line) and increases in size with γ; when $\gamma \geq \gamma_u \approx 0.2$, no metastable states remain.

in maintaining cell-cell contacts[34].

The effect of activity or thermal excitation of MS near the ground state is harder to evaluate, as a rigorous connection between inherent-state energies and energy barriers has not been established in general. Recent studies of thermally excited vertex and Voronoi models[35] use a description of excitation energies by spectra of collective vibrational modes, whose connection to the current formalism using statistical moments would be interesting to establish.

Further analytical predictions can be made from (8): The minimum (ground state) energy follows directly as

$$\varepsilon_f^{min} = 1 + M_{20}\mu_{20}(c_A) - M_{11}\mu_{11}^{max}(c_A)\,, \qquad (9)$$

which Fig. 3c shows is an excellent estimate for the lowest MS energies from simulations. Empirically, the ratio $\varepsilon_f^{max}(c_A)/\varepsilon_f^{min}(c_A) \approx 1.045$ of maximum to minimum foam energy found for the monodisperse case remains the same independent of polydispersity (Fig. 3c). This same estimate of maximum energy, through (8), also provides a linear boundary to the region of possible MS in the $\mu_{20} - \mu_{11}$ plane; together with the other phase boundaries, this estimate delineates the entire MS region (Fig. 2d).

The region of all metastable states is thus analytically defined as an area in $\mu_{20} - \mu_{11}$ space, and the foam or equivalent foam energies of these states are well predicted by a linear relation over that space. Actual energies of tissues or spring systems for known energy functionals can be recovered from ε_f^*, but even if the functional is not known, the size-topology parameters μ_{20} and μ_{11} provide an excellent prediction for the relative position of the system between the minimum and maximum possible MS energies.

The relation (8) also provides a more general view of the loss-of-rigidity transition in tissue systems: Both the criterion $\gamma > \gamma_c$ for floppy ground states[9] and the equivalent $\bar{p} > \bar{p}_c$ for the shape index $\bar{p} = (1/N)\sum_i P_i/\sqrt{A_i}$[7,36] are conditions on average perimeter length, and thus equivalent foam energy. Under mild assumptions of unimodality for the area distribution, we can therefore directly translate the critical shape index into a critical equivalent foam energy

$$\varepsilon_{f,c}^*(c_A) \approx (1+\gamma/2)c_A(\pi/2)^{1/2}3^{-1/4}\Gamma(c_A^{-2}+1/2)/\Gamma(c_A^{-2})\,, \qquad (10)$$

see Supplementary Information. However, long perimeters and thus large ε_f^* values can also occur in the (more energetic, rigid) metastable states. The MS energy prediction answers the question whether states of high shape index are actually floppy: If (8) predicts $\varepsilon_f^* < \varepsilon_{f,c}^*$, but an actual perimeter measurement shows $\varepsilon_f^* \approx \varepsilon_{f,c}^*$, the system is in a degenerate ground state. However, if $\varepsilon_f^* > \varepsilon_{f,c}^*$ is predicted in agreement with measurements, the large shape index instead indicates a rigid high-energy MS. This is illustrated for tissues with $\gamma > \gamma_c$ in Fig. 4a (monodisperse) and b ($c_A = 0.4$ polydisperse), respectively. The gray solid lines are given by $\varepsilon_f^* = \varepsilon_{f,c}^*$, separating the simulated floppy and rigid states. Evidently, there exists a *second* critical $\gamma = \gamma_u$ beyond which the set of degenerate ground states engulfs the entire MS region. Setting $\varepsilon_f^{*max}(c_A) = \varepsilon_{f,c}^*(c_A)$ implies a nearly constant $\gamma_u \approx 0.195...0.205$ in the range $c_A \leq c_A^{max}$. Beyond γ_u, tissue systems are *unconditionally* floppy/fluid.

6 Conclusions

The present work quantifies the metastable-state mechanical energy of a wide variety of 2D cellular systems as a universal function of moments of the size-topology distribution. It thus generalizes the unified use of size-topology correlations for the classification of ground states[37] to include the entirety of MS, a much larger state space. Remarkably, the universal MS energy (8) is a formal analog to linear elasticity: it is a quadratic functional of averaged "displacements" $A_i - \bar{A}$ and $n_i - \bar{n}$, evaluated locally at each domain. Although changes between metastable states involve the traversing of energy barriers and thus nonlinear and dissipative processes, the eventual changes in $\mu_{20} - \mu_{11}$ space can be described by linear moduli. Unlike classic elasticity, none of the moduli are independent: The geometric constraints of space filling restrict domain patterns so tightly that the relation can be derived from the simplest of structural examples, and the constraints are so universally active that the simple linear expression is accurate for the *entirety* of the MS space, independent of simulation protocols and across widely different energy functionals.

The practical relevance of this simple relation is that mechani-

cal energy values can be straightforwardly quantified from a snapshot of e.g. an emulsion, a superlattice domain material, or a biological tissue layer. Regions with more "unfavorable" statistics indicate mechanical weakness; in biological tissues, the approach could aid diagnostics of pathological or morphogenetic changes that affect mechanical functionality, and thus advance our understanding of tissue development and therapy.

Conflicts of interest

There are no conflicts to declare.

Acknowledgements

The authors are grateful for inspiring discussions with L. Manning, S. Torquato, and M. Bowick. SK acknowledges support by the NSF under grant #1504301.

Notes and references

1 D. Weaire and N. Rivier, *Contemporary Physics*, 1984, **25**, 59–99.
2 L. J. Gibson, M. F. Ashby and B. A. Harley, *Cellular materials in nature and medicine*, Cambridge University Press, 2010.
3 S. Torquato, *Random heterogeneous materials: microstructure and macroscopic properties*, Springer Science & Business Media, 2013, vol. 16.
4 P. Teixeira, F. Graner and M. Fortes, *The European Physical Journal E*, 2002, **9**, 161–169.
5 L. Ci, L. Song, C. Jin, D. Jariwala, D. Wu, Y. Li, A. Srivastava, Z. Wang, K. Storr, L. Balicas *et al.*, *Nature materials*, 2010, **9**, 430.
6 K. Novoselov, A. Mishchenko, A. Carvalho and A. C. Neto, *Science*, 2016, **353**, aac9439.
7 D. Bi, J. H. Lopez, J. M. Schwarz and M. L. Manning, *Nat Phys*, 2015, **11**, 1074–1079.
8 D. Bi, X. Yang, M. C. Marchetti and M. L. Manning, *Physical Review X*, 2016, **6**, 021011.
9 S. Kim and S. Hilgenfeldt, *Soft Matter*, 2015, **11**, 7270–7275.
10 M. P. Miklius and S. Hilgenfeldt, *Phys. Rev. Lett.*, 2012, **108**, 015502.
11 S. Kim, M. Cai and S. Hilgenfeldt, *New Journal of Physics*, 2014, **16**, 015024.
12 Images from the authors' group and, in case of the epithelial tissue, with permission of R. Carthew.
13 G. Zhang, F. Stillinger and S. Torquato, *Physical Review E*, 2017, **96**, 042146.
14 T. C. Hales, *Discrete & Computational Geometry*, 2001, **25**, 1–22.
15 F. H. Stillinger and T. A. Weber, *Science*, 1984, **225**, 983–989.
16 H. Makse, J. Brujic and S. F. Edwards, in *Statistical Mechanics of Jammed Matter*, Wiley-VCH Verlag GmbH Co. KGaA, 2005, pp. 45–85.
17 A. J. Liu and S. R. Nagel, *Nature*, 1998, **396**, 21.
18 S. Torquato and F. H. Stillinger, *Reviews of modern physics*, 2010, **82**, 2633.
19 S. Kim, Y. Wang and S. Hilgenfeldt, *Physical Review Letters*, 2018, **120**, 248001.
20 M. Krajnc, S. Dasgupta, P. Ziherl and J. Prost, *arXiv preprint arXiv:1805.06500*, 2018.
21 D. Staple, R. Farhadifar, J. C. Röper, B. Aigouy, S. Eaton and F. Jülicher, *The European Physical Journal E: Soft Matter and Biological Physics*, 2010, **33**, 117–127.
22 S. Kim, J. J. Cassidy, B. Yang, R. W. Carthew and S. Hilgenfeldt, *Biophysical Journal*, 2016, **111**, 2735 – 2746.
23 J.-A. Park, J. H. Kim, D. Bi, J. A. Mitchel, N. T. Qazvini, K. Tantisira, C. Y. Park, M. McGill, S.-H. Kim, B. Gweon *et al.*, *Nature materials*, 2015, **14**, 1040.
24 K. Brakke, *Experimental Mathematics*, 1992, **1**, 141–165.
25 V. Lucarini, *Journal of Statistical Physics*, 2008, **130**, 1047–1062.
26 S. Lloyd, *IEEE Trans. Inf. Theor.*, 2006, **28**, 129–137.
27 H. X. Zhu, S. M. Thorpe and A. H. Windle, *Philosophical Magazine A*, 2001, **81**, 2765–2783.
28 M. Durand and H. A. Stone, *Physical review letters*, 2006, **97**, 226101.
29 F. Graner, Y. Jiang, E. Janiaud and C. Flament, *Physical Review E*, 2000, **63**, 011402.
30 J. E. Taylor, *Annals of Mathematics*, 1976, 489–539.
31 P. Billingsley, *Convergence of probability measures*, John Wiley & Sons, 2013.
32 D. Bi, J. H. Lopez, J. M. Schwarz and M. L. Manning, *Soft Matter*, 2014, **10**, 1885–1890.
33 A. Mongera, P. Rowghanian, H. J. Gustafson, E. Shelton, D. A. Kealhofer, E. K. Carn, F. Serwane, A. A. Lucio, J. Giammona and O. Campàs, *Nature*, 2018, **561**, 401–405.
34 A. Sumi, P. Hayes, A. D'Angelo, J. Colombelli, G. Salbreux, K. Dierkes and J. Solon, *Developmental Cell*, 2018, **47**, 453 – 463.e3.
35 Sussman, Daniel M., Paoluzzi, M., Cristina Marchetti, M. and Lisa Manning, M., *EPL*, 2018, **121**, 36001.
36 M. Moshe, M. J. Bowick and M. C. Marchetti, *Physical Review Letters*, 2018, **120**, 268105.
37 K. Newhall, L. Pontani, I. Jorjadze, S. Hilgenfeldt and J. Brujic, *Physical Review Letters*, 2012, **108**, 268001.

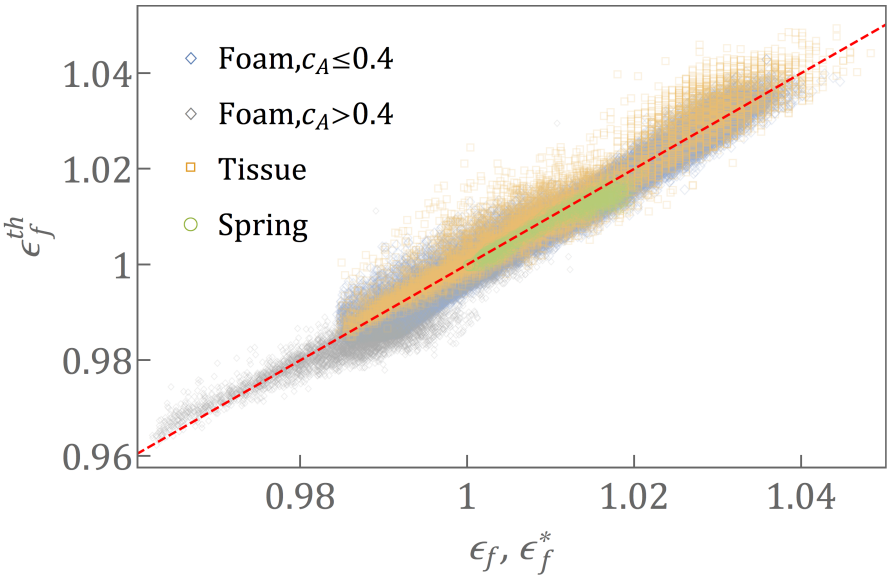

A linear theory accurately predicts the entire range of metastable state energies in diverse soft matter and biological cellular systems.